Appl. Phys. B 50, 137–144 (1990)

Applied Physics B Photophysics and Laser Chemistry

Sensitive Intracavity Photoacoustic Measurements with a CO_2 Waveguide Laser

F. J. M. Harren[1], F. G. C. Bijnen[1], J. Reuss[1], L. A. C. J. Voesenek[2], and C. W. P. M. Blom[2]

[1] Fysisch Laboratorium, Katholieke Universiteit Nijmegen, Toernooiveld, NL-6525 ED Nijmegen, The Netherlands
[2] Experimentele Plantkunde, Katholieke Universiteit Nijmegen, Toernooiveld, NL-6526 ED Nijmegen, The Netherlands

Received 20 March 1989/Accepted 24 June 1989

Abstract. A photoacoustic intracavity configuration is presented; a resonant photoacoustic cell excited in its first longitudinal mode is placed inside the cavity of a CO_2 waveguide laser. Due to the high laser power and the sharp intracavity focus, saturation effects occur in the excitation and relaxation process of absorbing C_2H_4 molecules. A more optimal configuration is applied to measure the C_2H_4 emission of several *Rumex* species. A detection sensitivity of 6 ppt (parts per trillion) C_2H_4 is reached, equivalent to a minimal detectable absorption of $1.8 \times 10^{-10}\,cm^{-1}$.

PACS: 07.60, 43.85, 42.60

The photoacoustic technique for trace gas detection has proved to be a sensitive and reliable method at wavelengths in the infrared and near infrared [1–6]. For practical applications, however, the photoacoustic method becomes significantly more interesting when its sensitivity exceeds – by some orders of magnitude – that of current conventional techniques such as a gas chromatograph equipped with a flame ionization detector or photoionization detector [7]. Inserting a photoacoustic cell in the laser cavity results in a photoacoustic detection which becomes even more sensitive due to the high intracavity laser power. Resonant photoacoustic cells for intracavity laser operation are known [8–12]. They combine a high sensitivity with a small length, necessary for intracavity operation.

However, the large volume of a resonant cell, operating at its lowest radial or azimuthal acoustical mode, is disadvantageous. The requirements for practical operation are usually a low gas consumption and a fast response [10]. An open resonant cell excited in its first longitudinal mode fulfills these requirements. It becomes possible to investigate the gaseous exudates of small biological samples, which are present as trace gas in ambient air.

In this paper we present such a photoacoustic cell placed inside the cavity of a CO_2 waveguide laser. We describe the development of the device for three intracavity configurations. As an application, the detection of C_2H_4 at ppt level (parts per trillion, $1{:}10^{12}$) will be discussed and measurements will be presented on the C_2H_4 emission of small *Rumex* plants (fresh weight ± 1 gram, 19 days old) under the stress of inundation.

1. Outline of the Intracavity Set-Up

The laser used is a CO_2 waveguide laser which emits radiation at wavelengths between 9 and 11 μm. The vibrational P and R transitions of CO_2 produce radiation in four branches yielding about 90 laser lines. A hollow dielectric waveguide tube of quartz permits transmission of the electromagnetic radiation with very small attenuation [13]. The waveguide tube has a inner diameter of 2.6 mm and a discharge length of 45 cm. An increased gain per unit length and a decreased physical size are advantages of operating a CO_2 waveguide laser instead of a normal CO_2 laser. The losses due to coupling the radiation from the waveguide into free space and back into the guide have

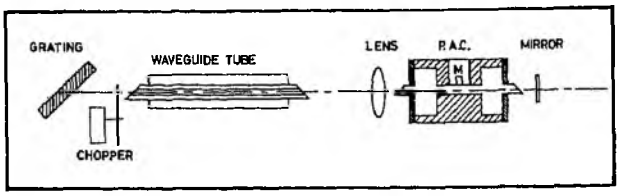

Fig. 1. General scheme of the photoacoustic intracavity measurement with a CO_2 waveguide laser (PAC photoacoustic cell, M microphone)

been discussed by Abrams and Mills [14, 15]. They have calculated that a minimum of losses occurs when the waist of the laser beam, compared to the radius of the waveguide tube has a ratio of 0.6435 ± 0.0002; 99% of the EH_{11} propagation mode inside the guide tube will be transferred into the TEM_{00} propagation mode of the free space. With this waveguide diameter dependent beam waist (w_0) we can describe the shape of the Gaussian laser beam inside the laser cavity, following the treatment of Kogelnik [16] for a Gaussian beam and its interaction with optical elements. The following equations (1 and 2) govern the radius of curvature of the wavefront R and the laser beam radius w as a function of the distance z from the beam waist w_0 (w is defined as the distance from the laser axis where the electric field amplitude has decreased to 1/e of its value on the axis).

$$R(z) = z\left[1 + \left(\frac{A}{z}\right)^2\right] \tag{1}$$

$$w(z) = w_0\left[1 + \left(\frac{z}{A}\right)^2\right]^{1/2} \quad \text{with} \quad A = \frac{\pi w_0^2}{\lambda}, \tag{2}$$

w_0 stands for the beam waist and λ for the optical wavelength. When a thin lens is inserted in a Gaussian beam, the transformation of the beam waist w_0 to w_1 and the distance of the new beam waist are

$$w_1 = w_0\sqrt{\frac{d_2 - f}{d_1 - f}}, \tag{3}$$

$$d_2 = f\frac{d_1(d_1 - f) + A^2}{(d_1 - f)^2 + A^2} \quad \text{with} \quad A = \frac{\pi w_1^2}{\lambda}, \tag{4}$$

f is the focal length of the lens, d_1 the distance from the first waist to the lens and d_2 the distance from the lens to the next waist. From these equations we can construct an intracavity set-up if the matching conditions at the end of the laser cavity are fulfilled. The beam radius $w(z)$ and the radius of curvature $R(z)$ of the wavefront must be equal for the forward and backward propagating beam at any point in the laser. Therefore, the curved end mirror must be placed at the distance z at which its curvature equals that of the wavefront. If we fulfill this condition any laser cavity configuration can be introduced. For the construction of the intracavity laser we used the experience gained with the construction of conventional cw CO_2 waveguide lasers [17]. Figures 1 and 2 show the intracavity arrangement for several experiments. The high-voltage dc discharge waveguide tube has an inner diameter of 2.6 mm, yielding a beam waist of 0.837 mm at the end of the tube ($w_0 = 0.6435\, t_{tube}$). The laser operates on a flowing CO_2, N_2, He gas mixture, which enters the tube near the window holders and leaves it at the high-voltage electrode at the centre. Deposition of small particles near the ZnSe Brewster windows and consequent distortion of the intracavity operation is thus prevented. The laser cavity is mounted on a frame of 3 invar rods, each of 18 mm diameter and 1.4 m long, connected by 5 aluminium plates to increase the rigidity of the construction. One end mirror is a grating blazed at 10.6 μm (150 l/mm, mounted on a PZT); the other end mirror is an exchangeable curved ZnSe window, one side is anti-reflection coated, the other side coated to high reflection (> 90%). This end mirror can be moved along the invar rods to change the length of the intracavity set-up.

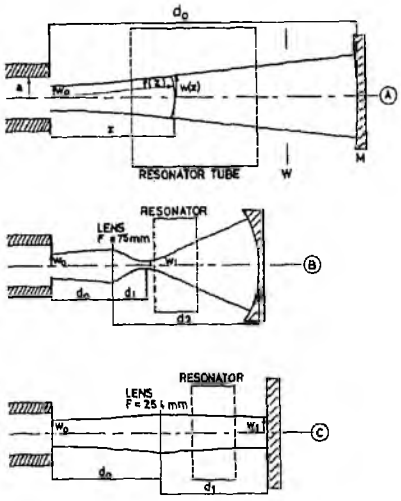

Fig. 2A–C. Laser beam parameters between waveguide tube (radius a) and end mirror (M) in the three different configurations. The acoustic resonator is drawn on scale in the set-up. **A** With curved end mirror ($R = 750$ mm) and without lens; **B** with lens ($f = 75$ mm) and curved end mirror ($R = 270$ mm); **C** with lens ($f = 254$ mm) and flat end mirror $R = \infty$)

The first photoacoustic intracavity experiments are done with a modulated discharge current. For varying laser power, however, large dc current variations interrupt the discharge. Therefore, a small mechanical chopper (85 mm blade diameter) is placed inside the laser cavity for modulation. The chopper is placed on rubber to minimize vibrational interference with the photoacoustic cell. To avoid light scattered and diffracted from the edges of the chopper blades entering the photoacoustic cell, the chopper is placed at the

grating side of the waveguide tube; the acoustic cell is placed at the mirror side. An additional advantage is the easier manipulation of the photoacoustic cell inside the laser cavity. Due to the shortened length of the acoustic resonator (as described later) a high frequency chopper blade is necessary (up to 2 kHz, 40 vanes). The laser-beam diameter becomes large in comparison with the small opening between two chopper vanes (ratio 1:2). If the chopper is operated inside the laser cavity a threefold reduction of the dc laser power is observed. An asymmetric chopper blade (more open than closed) could be used to recover an on/off ratio of the laser action to 1. This would ensure that the full modulated laser power is active to produce photoacoustic signal at the modulation frequency.

The photoacoustic cell is placed inside the laser cavity at the side of the end mirror permitting direct measurements of the laser power transmitted through the acoustic cell. If the cell was placed at the other side of the gain tube or if the power was measured at the side of the grating amplification of the laser beam intensity, due to another pass through the gain medium, could give a mismatch between the actual and measured laser power.

The discharge tube, photoacoustic cell and optic elements are aligned using a He–Ne laser. Final adjustment is made for maximum laser power. The laser power measured outside the laser cavity is multiplied by $2/T$(T the transmission of the end mirror) to calculate the intracavity laser power (i.e. in the order of 10^2 W).

2. First Experimental Set-Up

The first photoacoustic configuration is employed with the acoustic cell described elsewhere [17]. The resonant cell consists of a long cylindrical resonator tube (9 mm diameter, 300 mm long) inside a larger tube (58 $\times$ 450 mm^2). The cell has a resonant frequency at 560 Hz with a quality factor $Q=20.0$. The ZnSe windows at the ends of the outher tube are placed at Brewster angle. The ac pressure amplitude induced by the absorption of the modulated CO_2 laser radiation, is measured by 4 microphones (Knowles electret BT 1754, 10 mV/Pa sensitivity each) mounted circumferentically at the center of the resonator tube. The "extracavity" performance of the cell is listed in Table 1.

Because of the length of the photoacoustic cell (500 mm) we have chosen for a large radius of curvature of the end mirror ($R=750$ mm). The matching conditions are fulfilled for the radius of curvature of the laser beam wavefront at a distance of 670 mm. The laser beam radius (w) at the end of the acoustic resonator tube is 2.0 mm ($z=450$ mm). This was expected to be small enough to avoid interaction with the wall of the acoustic resonator (9 mm diameter). However, interference does occur near the 25 mm diameter ZnSe Brewster window. The passage hole through the window holder (7 mm diameter) causes a high photoacoustic background signal (48 μV/W, see Table 1) during measurements with highly purified N_2 (>99.995%). Together with the intracavity laser power (60 W) this yields a background signal of 2.9 mV. The background signal fluctuates with changes in the cavity (i.e., frequency tuning with the grating), which causes a decrease of sensitivity. A lower limit of absorption of 3×10^{-8} cm^{-1} is reached for the total set-up; with no background interference a lower limit of 1.1×10^{-10} cm^{-1} should be possible theoretically (60 W laser power, 1 μV/$\sqrt{\text{Hz}}$ background noise).

Thus a different intracavity set-up is needed to avoid high background signals; the radius (w) of the laser beam should be small as compared to the acoustic resonator tube and its window holders. Further, a decrease in length of the photoacoustic cell (i.e., decrease in laser cavity length) permits a more rigid construction of the laser. This results in the construction of a different configuration with an intracavity lens and a new small size photoacoustic cell.

Table 1. Characteristics of the laser cavity and the photoacoustic cell in its first configuration (Fig. 2a)

Laser configuration	
Beam waist near the waveguide tube	$w_0=0.836$ mm
Distance waveguide tube – end mirror	$d_0=690$ mm
Radius of curvature end mirror	$R=750$ mm
Largest laser beam radius inside the acoustic resonator	$w=2.0$ mm
Photoacoustic cell (4 microphones, 10 mV/Pa sensitivity each)	
Resonator length	300 mm
Resonator diameter	9 mm
Buffer length	75 mm
Buffer diameter	58 mm
Extracavity performance	
Acoustic background noise	1 μV/$\sqrt{\text{Hz}}$
Photoacoustic background signal	14 μV/W
Resonance frequency	560 Hz
Quality factor	20.0 ± 0.8
Cell constant (F)	$(4.0 \pm 0.2) \times 10^3$ Pa cm/W
Sensitivity of the cell (1 W laser power)	6.4×10^{-9} cm^{-1}
Intracavity performance	
Intracavity laser power	60 W
Photoacoustic background signal	48 μV/W
Sensitivity of the system	3.0×10^{-8} cm^{-1}

3. Laser Operation with an Intracavity Focus

3.1. The Small Size Photoacoustic Cell

A cell with a reduced length was made of aluminium containing a 100 mm long brass tube which acts as a resonator diameter 6 mm). The resonator is excited in its first longitudinal mode. Therefore, the end sections of the resonator are open and coupled to the buffer volumes (Fig. 3) (20 mm diameter, 50 mm long each). The buffer length (1/2 of the resonator length) is chosen such as to minimize the acoustic background signal originating from the absorption by the ZnSe windows. For the same reason the distance between the Brewster window and the acoustic buffer is chosen much smaller than 1/2 of the resonator length. The cell is equipped with one Knowles BT 1754 miniature electret microphone. It is coupled to the resonator through a 1.4 mm diameter hole in the tube wall.

The photoacoustic cell characteristics are given in Table 2. Acoustic resonance occurs at 1653 Hz with a quality factor $Q=31.8$ yielding a cell constant $F=3700$ Pa cm/W. The cell constant (F) and the quality factor (Q) depend on the geometry, the radius (r) and the length (l) of the resonant cell [18]. The cell constant (F) is the proportionality constant between the generated pressure amplitude p [Pascal] and the absorption coefficient of the gas α [atm^{-1} cm^{-1}, 1 atmosphere pressure] and the laserpower I_L [W].

For a longitudinal resonator $F \propto \sqrt{l}/r^{-1}\sqrt{l}$ and $Q \propto r/\sqrt{l}$, with $p=F\cdot\alpha\cdot I_L$. Due to its smaller length the value of the cell constant (F) is decreased in comparison with the first used long cell (Tables 1 and 2); the better experimental Q-value for the new cell partially compensates this difference.

Thus, a small size photoacoustic cell is designed with a volume of 35 cm^3. This is significally smaller than the 1200 cm^3 for the first cell and with practically no loss in experimental sensitivity.

3.2. The Second Intracavity Set-Up

To reduce the laser beam radius (w) compared to the cross dimensions of the photoacoustic cell we focus the laser beam (Fig. 2b) with a ZnSe lens (focal length 75 mm, both sides anti-reflection coated, at a distance of 150 mm from the waveguide tube). The end mirror is placed at the distance of 352 mm from the lens (radius of curvature 270 mm, reflection of 98.5%); the waist of the laser beam is observed at 84 mm distance from the lens at the entrance of the acoustic resonator tube. The largest laser beam radius inside the acoustic resonator amounts to 1.37 mm; this is small enough to move the photoacoustic cell slightly transverse to the laser beam without significant change of background signal (1.5 μV/W).

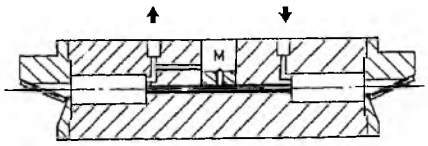

Fig. 3. Resonant photoacoustic cell used in the intracavity set-up of Figs. 2b and c. (Resonator: length 100 mm, diameter 6 mm. Buffer: length 50 mm, diameter 20 mm)

Table 2. Characteristics of the laser cavity and the new photoacoustic cell in the second configuration (Fig. 2b)

Laser configuration	
Beam waist near the waveguide tube	$w_0=0.836$ mm
Distance waveguide tube – lens	$d_0=150$ mm
Focal length lens	$f=75$ mm
Distance lens – end mirror	$d_2=352$ mm
Radius of curvature end mirror	$R=270$ mm
Beam waist between lens and end mirror	$w_1=0.282$ mm
Distance lens – second beam waist	$d_1=84$ mm
Largest laser beam radius inside the acoustic resonator	$w=1.37$ mm
Photoacoustic cell (1 microphone, 10 mV/Pa sensitivity)	
Resonator length	100 mm
Resonator diameter	6 mm
Buffer length	50 mm
Buffer diameter	20 mm
Extracavity performance	
Acoustic background noise	$0.5\,\mu\text{V}/\sqrt{\text{Hz}}$
Photoacoustic background signal	1.5 μV/W
Resonance frequency	1653 Hz
Quality factor	31.8 ± 0.8
Cell constant (F)	$(3.7\pm0.2)\times10^3$ Pa cm/W
Sensitivity of the cell (1 W laser power)	1.4×10^{-8} cm^{-1}
Intracavity performance	
Intracavity laser power	130 W
Photoacoustic background signal	1.5 μV/W
Sensitivity of the system	2.3×10^{-10} cm^{-1}

The results of the intracavity operation are listed in Table 2. The sensitivity of the intracavity set-up is tested with a trace of C_2H_4 in pure N_2 gas. C_2H_4 has a strong vibrational absorption (ν_7 vibration) at the 10P14 laser line of the CO_2 laser (absorption coefficient of 30.4 atm^{-1} cm^{-1} at 949.479 cm^{-1}) [19] and weaker absorptions at the 10P12 and 10P16 CO_2 laser transitions (4.35 atm^{-1} cm^{-1}, 951.192 cm^{-1} and 5.06 atm^{-1} cm^{-1}, 947.741 cm^{-1}, respectively). By measuring the photoacoustic signal on these laser lines with a known concentration of trace gas the sensitivity of the photoacoustic cell can be defined. However, the

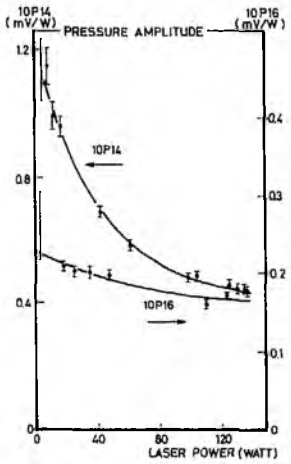

Fig. 4. The photoacoustic pressure amplitude as a function of the intracavity laser power for a strong (10*P*14, left ordinate) and a weaker (10*P*16, right ordinate) absorption of C_2H_4 at CO_2 laser lines. Due to the strong intracavity focus ($w=0.282$ mm) the transition saturates already at low laser power for the strong absorption; the weaker absorption does not show such a strong decrease

intracavity response was found not to be in agreement with the measurements performed in an extracavity set-up (Fig. 4). Extracavity, the ratio between the 10*P*14 and 10*P*16 CO_2 laser line is 6.0 ± 0.7 [19]; intracavity this ratio becomes 2.8 ± 0.3 at an intracavity laser power of 130 W. By lowering the intracavity laser power this ratio increases to its extracavity value. This effect is caused by saturation of the transitions in C_2H_4 at the 10*P*14 CO_2 laser line. The depletion from the vibrational excited level (v_7) via other vibrational levels (e.g., v_{10}) through collisions becomes slow in comparison with the pump rate due to the high intracavity power (130 W).

4. Third Experimental Set-Up

In our third configuration we have chosen for a larger beam waist in the focus after the lens to reduce the saturation effect. A ZnSe lens with a larger focal length ($f=254$ mm) is placed at $d_1=260$ mm from the waveguide tube. If we choose $d_1=f$ we obtain a maximum value for the second beam waist ($w_1=1.02$ mm). We are now able to place a flat end mirror (92.1% reflection) in this focus, leaving enough space for the acoustic cell. The distance lens-end mirror is not critical for laser action due to the slow variation of the radius of our curvature of beam propagation in the focus. In this configuration the intracavity power is about 100 W; the results of the set-up are listed in Table 3. The background signal remains at a low value (1.5 μV/W), in spite of the increased beam waist. The respons of the intracavity acoustic signal as a function of the laser power is given in Fig. 5. The ratio between

Table 3. Characteristics of the laser cavity and the new photoacoustic cell in the third set-up (Fig. 2c)

Laser configuration	
Beam waist near the waveguide tube	$w_0=0.836$ mm
Distance waveguide tube – lens	$d_0=260$ mm
Focal length lens	$f=254$ mm
Distance lens – end mirror	$d_2=263$ mm
Radius of curvature end mirror	$R=\infty$
Beam waist between lens and end mirror	$w_1=1.02$ mm
Distance lens – second beam waist	$d_1=263$ mm
Largest laser beam radius inside the acoustic resonator	$w=1.18$ mm
Photoacoustic cell (1 microphone, 10 mV/Pa sensitivity)	
Resonator length	100 mm
Resonator diameter	6 mm
Buffer length	50 mm
Buffer diameter	20 mm
Extracavity performance	
Acoustic background noise	$0.5\,\mu V/\sqrt{Hz}$
Photoacoustic background signal	1.5 μV/W
Resonance frequency	1653 Hz
Quality factor	31.8 ± 0.8
Cell constant (F)	$(3.7\pm0.2)\times10^3$ Pa cm/W
Sensitivity of the cell (1 W laser power)	1.4×10^{-8} cm^{-1}
Intracavity performance	
Intracavity laser power	100 W
Photoacoustic background signal	1.5 μV/W
Sensitivity of the system	1.8×10^{-10} cm^{-1}

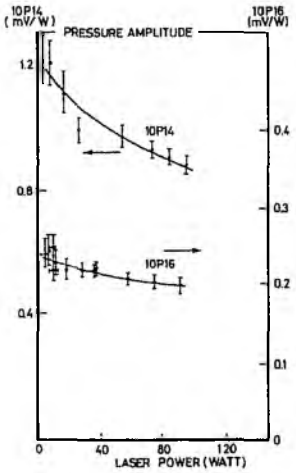

Fig. 5. The photoacoustic pressure amplitude versus the laser power; due to the less sharp focus ($w=1.02$ mm) the transition on the 10*P*14 CO_2 laser line saturates much less (78% at full intracavity power of 100 W)

the absorption coefficients of C_2H_4 on the 10*P*14 and 10*P*16 CO_2 laser lines is increased to 78% of its extracavity value (10*P*14/10*P*16 = 4.7 ± 0.5).

With this laser configuration we have measured the C_2H_4 emission of small inundated plants to utilize the improved detection limit of the intracavity set-up. We have taken an absorption coefficient of 23.7 $atm^{-1}\,cm^{-1}$ (78% of 30.4 $atm^{-1}\,cm^{-1}$ at an intracavity power of 100 W) of C_2H_4 on the 10*P*14 CO_2 laser line to correct for the saturation effect. A practical detection limit is reached of 6 ppt C_2H_4 in air, comparable to a sensitivity of $1.8 \times 10^{-10}\,cm^{-1}$.

5. Application

In The Netherlands the river areas are characterized by strongly changing water levels caused by irregular run off of rain and melting water. Flooding in summertime influences the distribution, the population biology and physiological processes of plants in these areas [20]. The zonation of *Rumex* species (Fig. 6) seems to be related to these irregular floodings during the growing season [21]; especially the frequency and duration of the floodings are important factors for the survival of the species. Plants occurring in the interface region between land and water must have developed adaptations to survive these conditions. One of the adaptations is a strong increase in growth of the shoot to restore contact of the leaves with the atmosphere. This enhanced growth of petioles or stems (up to 250% length increase in 96 h [22]) is partially regulated by the gaseous hormone ethylene (C_2H_4). The investigated species (*Rumex palustris*, *R. crispus* and *R. acetosa*) have different responses to inundation. *Rumex palustris* and *R. crispus* can enhance petiole growth in response to submergence, while *R. acetosa* has no increased growth of the petioles [23]. The different responses correlate very well with the location of the species in the field.

The diffusion rate of C_2H_4 in water is about 10,000 times slower than in air [24]; this causes an accumulation of C_2H_4 in the plant during submergence. An increase in the endogenous C_2H_4 level is found in all three *Rumex* species [22, 23]. Difference in growth responses under submerged conditions are therefore not related to differences in internal C_2H_4 concentrations but to differences in sensitivity to enhanced C_2H_4 levels. Partially submerged *Rumex* plants (shoot above water surface) also show elongation responses (*R. crispus* and *R. palustris*) and reduced petiole growth (*R. acetosa*). Probably these growth responses under waterlogged conditions are also regulated by ethylene. Increased levels of ethylene in the plant tissue during waterlogging can only be caused by increased ethylene production and not by accumulation in the

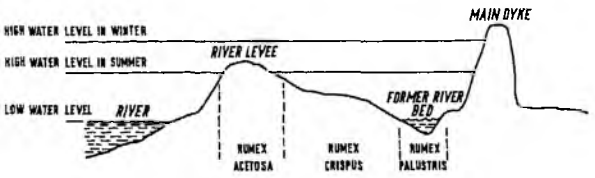

Fig. 6. The zonation of *Rumex* species in relation with the irregular flooding in the river areas during the growing season

plant. To study the C_2H_4 production under partially submerged conditions experiments with a continuous flow system and the photoacoustic detection technique were performed. The set-up of the gas handling system will be described elsewhere [17]; a short review follows below.

During the experiment two plants are placed in a small glass sample cell (200 cm^3, 25 °C, photon flux density 50 μEinstein/m^2s, 24 h a day; 1 Einstein = 6.02 × 10^{23} photons in the 400–700 nm wavelength region). After an adaption period (24 h) one plant is partially inundated while the other is grown under drained control conditions. To avoid accumulation of gases in ambient air, which can influence the C_2H_4 production rate, the sample cell with its inlet and outlet ports is connected to a continuous flow system (flow velocity 0.9 l/h). Before it enters the sampling cell the air is passed through a catalyst to remove hydrocarbon trace gases by converting them into H_2O and CO_2. This is necessary in order to avoid unwanted effects of these hydrocarbons on the biological samples. Between the sample cell and the photoacoustic cell a KOH based scrubber eliminates CO_2 and H_2O without influencing the C_2H_4 concentration. Despite the low concentration (330 ppm) and the weak absorption strength the CO_2 has exact coincidences with the vibrational laser transitions of the CO_2 laser, therefore it has to be removed to avoid interferences with C_2H_4 on the photoacoustic signal [5].

The phase of the photoacoustic signal, which is affected by CO_2 and H_2O absorption, can also be used to determine the C_2H_4 concentration without removing the CO_2 from the gasflow [25].

The removal time of the total gas content in the system is 4 min (1/e time). Figure 7 shows the measured C_2H_4 concentration increase compared to the reference plant and the calculated production rate of the three *Rumex* species as a function of time. The C_2H_4 concentration is calculated from the photoacoustic signal on the 10*P*14 (strong C_2H_4 absorption) and 10*P*12 (weaker C_2H_4 absorption) CO_2 laser lines. The C_2H_4 production rate (in nanoliter per gram dry weight per hour) on the right ordinate follows from the product of the C_2H_4 concentration (in ppb or nanol/l, left ordinate), the gas flow (l/h) and the dry weight (DW) of the plant. The production rate of the reference

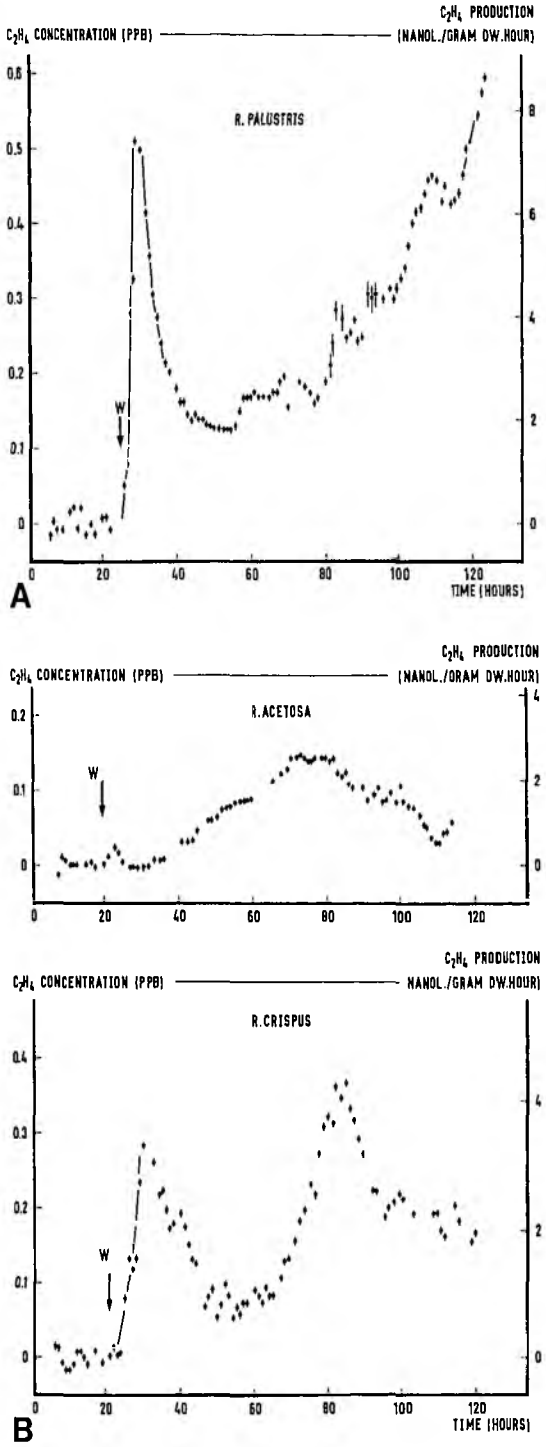

Fig. 7A, B. The increase of the ethylene production versus time is shown during partial inundation of three *Rumex* species: *Rumex palustris* (dry weight 0.062 g). *R. crispus* (d.w. 0.078 g) and *R. acetosa* (d.w. 0.051 g). The increase compared to a reference plant is shown. During the experiment the reference plant shows no significant increase in ethylene production. During the measured 96 h after waterlogging (marked with W) *R. palustris* and *R. crispus* show elongation of the youngest leaves; *R. acetosa* shows a reduced growth

plants was constant during the experiments (*R. acetosa* = 1.69 nanol/gram DWh; *R. crispus* = 0.63 nanol/gram DWh; *R. palustris* = 0.50 nanol/gram DWh) and subtracted from the production of the inundated species to show the increased production rate of Fig. 7. At the time markers water is added resulting in an increase of the C_2H_4 production. The possible influence of the soil and the water on the photoacoustic signal is tested in separate experiment and is found negligible. As depicted in Fig. 7, all three species show an increase of C_2H_4 production. A few hours after the onset of the flooding treatment a stress-induced increase is followed by a sharp decrease of the production. The next phase is characterized by a gradual increas again of the C_2H_4 production. *R. palustris* and *R. crispus* both show a strongly increased production relative to the control production which correlates with elongation of mainly the youngest petioles, an important adaptation to overcome aeration stress in the flooded soil. *R. acetosa*, which is not resistant to flooding and shows reduced growth if C_2H_4 is applied, reacts to flooding by a relatively small production of C_2H_4.

6. Conclusion

A photoacoustic intracavity configuration is described; a resonant acoustic cell is excited in its first longitudinal mode, inside the cavity of a CO_2 waveguide laser. Three intracavity configurations are discussed; the optimal third one is applied to measurements of emitted C_2H_4 from a biological sample. The second intracavity set-up, with the sharp intracavity focus is not suitable for measuring C_2H_4 concentrations due to the significant degree of saturation. However, it can still be a solution for other trace gases with a faster relaxation rate (e.g., NH_3). The less sharp focus of the third configuration prevents saturation sufficiently. Further increase of the reached minimum detectable absorption coefficient ($1.8 \times 10^{-10}\,cm^{-1}$) is possible with a more sensitive microphone (we worked with a microphone response of 10 mV/Pa) or by using more microphones.

However, with increased microphone sensitivity an active suppression of the acoustic room noise and the photoacoustic background signal from the windows (increased laser power) seems then to become necessary. A double resonant system, with two longitudinal resonator tubes placed parallel and near to each other can be a solution for this problem. The reference resonator measures the photoacoustic background signal from the windows and the possible acoustic room noise which can be subtracted from the acoustic signal from the sample resonator transversed by the laser beam.

Finally, in a flowing air system the ethylene production of partially inundated *Rumex* species is demonstrated. All three species show an increase in ethylene production compared to a reference plant which is correlated with an increased growth of the petioles with the exception of *R. acetosa* which shows a decrease in growth. During the experiment a practical detection limit of 6 ppt C_2H_4 is reached in purified air (other hydrocarbons are removed), comparable to a minimum detectable absorption coefficient of 1.8×10^{-10} cm^{-1} for the intracavity photoacoustic set-up.

References

1. V.P. Zharov, V.S. Letokhov: *Laser Opto Acoustic Spectroscopy*, Springer Ser. Opt. Sci. **37** (Springer, Berlin, Heidelberg 1986)
2. G.L. Loper, J.A. Gelbwachs, S.M. Beck: Can J. Phys. **69**, 1124 (1986)
3. H. Ahlberg, S. Lundqvist, S.T. Eng: Appl. Opt. **23**, 2902 (1984)
4. S.T. Bernegger, P.L. Meyer, C. Widmer, M.W. Sigrist: In *Photoacoustic and Photothermal Phenomena*, ed. by P. Hess and J. Pelzl, Springer Ser. Opt. Sci. **58**, (Springer, Berlin, Heidelberg 1987)
5. P. Perlmutter, S. Shtrikman, M. Slatkine: Appl. Opt. **18**, 2267 (1979)
6. R. Gerlach, N.M. Amer: Appl. Phys. Lett. **32**, 228 (1978)
7. D.K. Bassi, M.S. Spencer: Plant Cell Environm. **8**, 161 (1985)
8. R. Gerlach, N.M. Amer: Appl. Phys. **23**, 319 (1980)
9. K.P. Koch, W. Lahmann: Appl. Phys. Lett. **32**, 289 (1978)
10. S. Shtrikman, M. Slatkine: Appl. Phys. Lett. **31**, 830 (1977)
11. D.H. Leslie, G.L. Trusty: Appl. Opt. **20**, 1941 (1981)
12. J. Röper, G. Chen, P. Hess: Appl. Phys. B **43**, 57 (1987)
13. J.J. Degnan: Appl. Phys. **11**, 1 (1976)
14. R.L. Abrams: IEEE J. QE-**8**, 838 (1972)
15. C.A. Hill, D.R. Hall: Appl. Opt. **24**, 1283 (1985)
16. H. Kogelnik, T. Li: Proc. IEEE **54**, 1312 (1966)
17. F. Harren: To be published
18. S.D. Bernegger, M.W. Sigrist: Appl. Phys. B **44**, 125 (1987)
19. R.J. Brewer, C.W. Bruce, J.L. Mater: Appl. Opt. **21**, 4092 (1982)
20. C.W.P.M. Blom: Waarnemen en verklaren, een beschouwing over plantenoecologie, Inaugural Address, Brakkenstein, Nijmegen (1985)
21. L.A.C.J. Voesenek, C.W.P.M. Blom: Can. J. Botany **65**, 1638–1642 (1987)
22. L.A.C.J. Voesenek, C.W.P.M. Blom: Plant Cell Environm. **12**, L 43–439 (1989)
23. L.A.C.J. Voesenek, C.W.P.M. Blom: Ethylene and flooding responses of Rumex species, in *Biochemical and Physiological Aspects of Ethylene Production in Lower and Higher Plants*, ed. by H.C. Lijsters et al.: (Kluwer, Dordrecht 1989) pp. 245–253
24. M.B. Jackson: Ann. Rev. Plant Physiol. **36**, 145–174 (1985)
25. R.A. Rooth, A.J.L. Verhage, L.W. Wouters, L. van de Beld: Proc. 4th Int. Conf. on Infrared Physics, Zürich, Switzerland (1988) p. 593

Responsible for Advertisements: E. Lückermann, G. Probst, Heidelberger Platz 3, D-1000 Berlin 33, Tel. (030) 8207-0, Telex 01-85411, FAX (0) 30/8207300
Responsible for the Text: H. K. V. Lotsch, Tiergartenstrasse 17, D-6900 Heidelberg, Tel. (0) 6221/487253, Telex 461723, FAX (0) 6221/43982
Printers: Brühlsche Universitätsdruckerei, Giessen

Springer-Verlag GmbH & Co. KG, D-1000 Berlin 33